

# REPORT DOCUMENTATION PAGE

Form Approved  
OMB No. 0704-0188

Public reporting burden for this collection of information is estimated to average 1 hour per response, including the time for reviewing instructions, searching existing data sources, gathering and maintaining the data needed, and completing and reviewing this collection of information. Send comments regarding this burden estimate or any other aspect of this collection of information, including suggestions for reducing this burden to Department of Defense, Washington Headquarters Services, Directorate for Information Operations and Reports (0704-0188), 1215 Jefferson Davis Highway, Suite 1204, Arlington, VA 22202-4302. Respondents should be aware that notwithstanding any other provision of law, no person shall be subject to any penalty for failing to comply with a collection of information if it does not display a currently valid OMB control number. **PLEASE DO NOT RETURN YOUR FORM TO THE ABOVE ADDRESS.**

<b>1. REPORT DATE (DD-MM-YYYY)</b>		<b>2. REPORT TYPE</b>	<b>3. DATES COVERED (From - To)</b>		
<b>4. TITLE AND SUBTITLE</b>			<b>5a. CONTRACT NUMBER</b>		
			<b>5b. GRANT NUMBER</b>		
			<b>5c. PROGRAM ELEMENT NUMBER</b>		
<b>6. AUTHOR(S)</b>			<b>5d. PROJECT NUMBER</b>		
			<b>5e. TASK NUMBER</b>		
			<b>5f. WORK UNIT NUMBER</b>		
<b>7. PERFORMING ORGANIZATION NAME(S) AND ADDRESS(ES)</b>			<b>8. PERFORMING ORGANIZATION REPORT NUMBER</b>		
<b>9. SPONSORING / MONITORING AGENCY NAME(S) AND ADDRESS(ES)</b>			<b>10. SPONSOR/MONITOR'S ACRONYM(S)</b>		
			<b>11. SPONSOR/MONITOR'S REPORT NUMBER(S)</b>		
<b>12. DISTRIBUTION / AVAILABILITY STATEMENT</b>					
<b>13. SUPPLEMENTARY NOTES</b>					
<b>14. ABSTRACT</b>					
<b>15. SUBJECT TERMS</b>					
<b>16. SECURITY CLASSIFICATION OF:</b>			<b>17. LIMITATION OF ABSTRACT</b>	<b>18. NUMBER OF PAGES</b>	<b>19a. NAME OF RESPONSIBLE PERSON</b>
<b>a. REPORT</b>	<b>b. ABSTRACT</b>	<b>c. THIS PAGE</b>			<b>19b. TELEPHONE NUMBER (include area code)</b>

## Report Title

Growth and Optimization of InGaSb/AlGaSb Quantum-Well-Based VECSELs on GaAs/AlGaAs DBRs

### ABSTRACT

We report the growth of optically pumped vertical-external-cavity surface-emitting lasers (VECSELs) based on InGaSb/AlGaSb quantum wells grown on GaAs/AlGaAs distributed Bragg reflectors (DBRs). The 7.78% lattice mismatch between GaSb and GaAs is accommodated by an array of  $90^\circ$  misfit dislocations at the interface. This results in spontaneous relaxation of the GaSb epilayer and also significantly reduces the threading dislocation density. The VECSELs are operated in both pulsed (with 340-W peak output power) and continuous wave mode (with 0.12-W peak output power). We investigate the effects of the GaSb/GaAs interface by comparing the lattice mismatched III-Sb VECSEL grown on GaAs/AlGaAs DBRs to a lattice matched III-Sb VECSEL grown on GaSb/AlAsSb DBRs. The lattice matched VECSEL outperforms the lattice mismatched VECSEL in terms of threshold pump density, efficiency, and maximum continuous-wave output power. This can be attributed to the presence of threading dislocations throughout the active region of the mismatched VECSEL, which is confirmed by cross-sectional transmission electron microscopy. The optical properties of the III-Sb active regions are characterized by time-resolved photoluminescence, which can be used to optimize the IMF interface.

---

**REPORT DOCUMENTATION PAGE (SF298)**  
**(Continuation Sheet)**

---

Continuation for Block 13

ARO Report Number 60508.1-EL-REP  
Growth and Optimization of 2-D InGaS ...

Block 13: Supplementary Note

© 2013 . Published in IEEE Journal of Selected Topics in Quantum Electronics, Vol. Ed. 0 19, (4) (2013), (, (4). DoD Components reserve a royalty-free, nonexclusive and irrevocable right to reproduce, publish, or otherwise use the work for Federal purposes, and to authorize others to do so (DODGARS §32.36). The views, opinions and/or findings contained in this report are those of the author(s) and should not be construed as an official Department of the Army position, policy or decision, unless so designated by other documentation.

Approved for public release; distribution is unlimited.

# Growth and Optimization of 2- $\mu\text{m}$ InGaSb/AlGaSb Quantum-Well-Based VECSELS on GaAs/AlGaAs DBRs

Pankaj Ahirwar, Thomas J. Rotter, *Member, IEEE*, Darryl Shima, Nahid A. Jahan, Stephen P. R. Clark, Sadvikas J. Addamane, Ganesh Balakrishnan, *Member, IEEE*, Alexandre Laurain, Jörg Hader, Yi-Ying Lai, Jerome V. Moloney, Ikuo Suemune, and Robert G. Bedford

(Invited Paper)

**Abstract**—We report the growth of optically pumped vertical-external-cavity surface-emitting lasers (VECSELS) based on InGaSb/AlGaSb quantum wells grown on GaAs/AlGaAs distributed Bragg reflectors (DBRs). The 7.78% lattice mismatch between GaSb and GaAs is accommodated by an array of 90° misfit dislocations at the interface. This results in spontaneous relaxation of the GaSb epilayer and also significantly reduces the threading dislocation density. The VECSELS are operated in both pulsed (with 340-W peak output power) and continuous wave mode (with 0.12-W peak output power). We investigate the effects of the GaSb/GaAs interface by comparing the lattice mismatched III-Sb VECSEL grown on GaAs/AlGaAs DBRs to a lattice matched III-Sb VECSEL grown on GaSb/AlAsSb DBRs. The lattice matched VECSEL outperforms the lattice mismatched VECSEL in terms of threshold pump density, efficiency, and maximum continuous-wave output power. This can be attributed to the presence of threading dislocations throughout the active region of the mismatched VECSEL, which is confirmed by cross-sectional transmission electron microscopy. The optical properties of the III-Sb active regions are characterized by time-resolved photoluminescence, which can be used to optimize the IMF interface.

**Index Terms**—Semiconductor lasers, surface-emitting lasers, quantum-well lasers.

Manuscript received November 15, 2012; revised January 3, 2013; accepted January 8, 2013. This work was supported in part by the Air Force Office of Scientific Research under Grant FA9550-09-1-0202 and Grant FA9550-07-1-0573 and by the Department of Defense HBCU/MI grant W911NF-12-1-0058.

P. Ahirwar, T. J. Rotter, D. Shima, S. P. R. Clark, S. J. Addamane, and G. Balakrishnan are with the Center for High Technology Materials, The University of New Mexico, Albuquerque, NM 87106 USA (e-mail: panki@chtm.unm.edu; tjr@chtm.unm.edu; dmshima@unm.edu; zippy2@unm.edu; addamane@unm.edu; gunny@unm.edu).

A. Laurain, J. Hader, Y.-Y. Lai, and J. V. Moloney are with the College of Optical Sciences, University of Arizona, Tucson, AZ 85721 USA (e-mail: alaurain@email.arizona.edu; jhader@acms.arizona.edu; yylai@acms.arizona.edu; jml@acms.arizona.edu).

N. A. Jahan and I. Suemune are with the Research Institute for Electronic Science, Hokkaido University, Sapporo 001-0021, Japan (e-mail: nahidajahan@yahoo.com; isuemune@es.hokudai.ac.jp).

R. G. Bedford is with the Air Force Research Laboratory, Wright Patterson AFB, OH 45433 USA (e-mail: Robert.Bedford@wpafb.af.mil).

Color versions of one or more of the figures in this paper are available online at <http://ieeexplore.ieee.org>.

Digital Object Identifier 10.1109/JSTQE.2013.2239615

## I. INTRODUCTION

THE 2- $\mu\text{m}$  vertical-external-cavity surface-emitting laser (VECSEL) has applications in a variety of technologies from gas sensing to infrared counter measures. The use of antimonide semiconductors for lasers in the 1.8–3.3  $\mu\text{m}$  wavelength range is well established with a majority of such lasers fabricated as edge emitting diodes including distributed feedback lasers [1]. However, the high beam quality and large output power of the VECSEL could be considerably advantageous to antimonide lasers in this wavelength range.

The power scaling in a VECSEL is achieved by increasing the diameter of the pump spot while keeping the pump density constant. Quantum-well (QW) VECSELS based on InGaAs QWs grown on GaAs substrates have recently broken the 100-W barriers for continuous-wave (CW) output power from a single chip [2]. However, the same level of success has not been achieved with antimonide VECSELS, which have not yet reached 10-W CW. The main reason for the “order of magnitude” reduction in the maximum CW power achieved by VECSELS on GaAs- versus the GaSb-based lasers can be primarily attributed to thermal management issues. The InGaAs-based lasers are based on a mature substrate removal technology that permits the complete substrate removal, and therefore, the intracavity diamond heat spreader can be moved out of the cavity. Antimonides lack such effective etch stop layers, which have restricted these lasers to thermal management schemes that require intracavity heat spreading. The use of intracavity heat spreaders such as transparent diamond invariably leads to stimulated photons in the cavity interacting with defects in the diamond, enough to restrict the performance of the lasers. Thus, the ability to grow antimonide VECSELS on a substrate with an established etch stop recipe such as on GaAs or InP could lead to significant improvements in the thermal management of the antimonide lasers and, consequently, a much higher value for the maximum CW output power from the lasers.

One such strategy to achieve antimonide VECSELS on GaAs would be to develop the growth of antimonide active regions on GaAs substrates which would allow for complete substrate removal without the need for an etch stop layer. A citric-acid-based etch has a high selectivity between GaSb and GaAs and can thus result in complete removal of the substrate. However,

the main issue with this approach is the 7.78% mismatch that exists between the GaSb and the GaAs binaries, which could lead to extensive threading dislocations in the GaSb epilayer and hence result in overwhelming nonradiative recombination losses in the antimonide active region. Furthermore, if the growth of the antimonide active region is done on a GaAs substrate, the first QW is typically within 500 nm of the mismatched interface. Thus, apart from the issue of excessive threading dislocations, we must also address the issue of nonreproducible relaxation in the antimonide buffer. If the antimonide buffer does not relax reproducibly, then the in-plane lattice constant of the buffer will be changed from growth to growth, also affecting the QW strain between growths. Such issues lead to performance degradation in edge emitters; however, in a vertical cavity laser, the position of the gain peak and the microcavity resonance must be precise, and variation in the gain peak is much more catastrophic. Thus, any metamorphic buffer-based approach has to result in two conditions in the active region: 1) the antimonide layer should have the minimum possible threading dislocation density (TDD); and 2) the buffer must have a highly reproducible lattice constant with preferably a 100% relaxation.

In this body of research, we explore the ability to grow GaSb-based active regions directly on GaAs substrates by inducing an interfacial array of misfit dislocations (IMF). The study further investigates the ability to grow such active regions on GaAs/AlGaAs distributed Bragg reflector (DBR) to investigate the effects of the highly mismatched interface on the performance of the VECSEL. Finally, we conduct cross-sectional transmission electron microscopy (TEM) investigation of the VECSEL structures.

## II. EPITAXIAL GROWTH OF THE VECSELS

A VECSEL typically consists of a semiconductor gain mirror and an external mirror (also known as output coupler). The optical mode in the device forms a standing wave pattern between the two mirrors. The QWs in the gain medium need to be placed at the antinodes of the standing E-field for optimum device performance [3], [4]. This design is usually referred to as a Resonant Periodic Gain structure. The distance between the QW layers corresponds to an optical path length of  $\lambda/2$ ; with nine QWs, the total length of the III-Sb subcavity is roughly  $5\lambda$ . The subcavity length plays an important role in the pump absorption. The incident pump radiation is absorbed both by barriers and wells; however, the well thickness in the design is  $1/20$  times that of barrier; therefore, multiple QWs are required for lasing of the VECSEL device. Due to low gain from the thin QW active region, a high reflectivity  $R \sim 99\%$  is needed to achieve lasing [1].

The VECSEL devices discussed in this paper are comprised of an epitaxially grown III-Sb-based active region emitting at or near  $2 \mu\text{m}$  on GaAs/AlGaAs DBRs, which are compared to the same active region grown lattice matched to GaSb/AlAsSb DBRs. The gain is provided by nine QWs, each 13 nm wide  $\text{Ga}_{0.8}\text{In}_{0.2}\text{Sb}$  separated by 260.4 nm  $\text{Al}_{0.25}\text{Ga}_{0.75}\text{Sb}$  barriers. The active region and AlAsSb/GaSb DBR is epitaxially grown by elemental source molecular beam epitaxy (MBE) in a VG

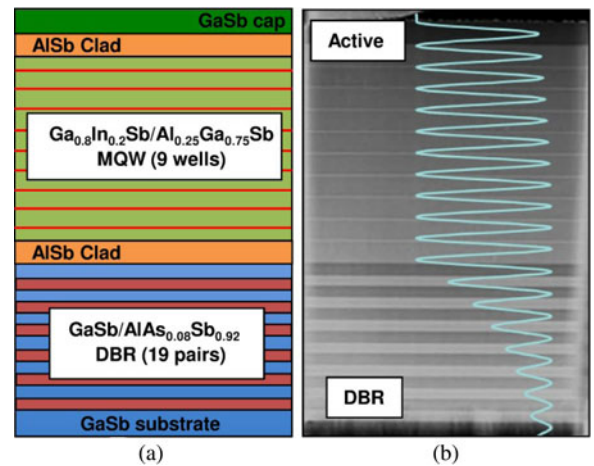


Fig. 1. (a) Schematic and (b) cross-sectional TEM image and plot of E-field for lattice matched  $2\text{-}\mu\text{m}$  III-Sb VECSEL grown on GaSb/AlAsSb DBR.

Semicon V80H reactor and in the case of the antimonide VECSEL on GaAs/AlGaAs DBRs the active region is MBE grown and the DBR is metal-organic chemical vapor deposition (MOCVD) grown. In the case of the all-antimonide VECSEL, the entire structure is lattice matched to the GaSb substrate, while in the case of the antimonide VECSEL on GaAs/AlGaAs, the active region has a lattice constant of  $6.09 \text{ \AA}$ , while the DBR is lattice matched to GaAs ( $a = 5.65 \text{ \AA}$ ). In this section, we shall discuss the designs of the all-antimonide lattice matched VECSEL and compare it to a design for an antimonide active-region-based VECSEL on a GaAs/AlGaAs DBR. We shall also discuss the growth strategies used to achieve an interfacial array of misfit dislocation at the GaSb/GaAs interface.

### A. $2\text{-}\mu\text{m}$ VECSEL Structure on GaAs/AlGaAs DBRs

Fig. 1(a) shows a schematic illustration of the fabricated VECSEL structure on a GaSb substrate. The bottom DBR is comprised of 19 pairs of  $\text{AlAs}_{0.08}\text{Sb}_{0.92}$  (153.8 nm)/GaSb (132.6 nm). The active region consists of nine  $\text{In}_{0.2}\text{Ga}_{0.8}\text{Sb}$  QWs separated by pump absorbing  $\text{Al}_{0.25}\text{Ga}_{0.75}\text{Sb}$  barriers. An AlSb confinement layer on each side of the active region ensures carrier confinement in the structure, and a thin GaSb capping layer is added on top to prevent oxidation. A low-resolution TEM image of the structure is shown in Fig. 1(b), the structure matches the epitaxially grown structure (only a few DBR pairs are captured in image). Fig. 1(b) also shows the E-field profile for the lattice matched VECSEL.

The schematic illustration, E-field profile, and low-resolution TEM image of the VECSEL structure grown on a GaAs substrate are shown in Fig. 2(a) and (b), respectively. The bottom DBR in this device consists of 25 pairs of  $\text{Al}_{0.95}\text{Ga}_{0.05}\text{As}$  (172 nm)/GaAs (149 nm) which is grown using MOCVD. The active region is then grown by MBE. It also consists of nine  $\text{In}_{0.2}\text{Ga}_{0.8}\text{Sb}$  QWs separated by pump absorbing  $\text{Al}_{0.25}\text{Ga}_{0.75}\text{Sb}$  barriers and AlSb top/bottom clad.

The key feature of the antimonide VECSEL based on the GaAs/AlGaAs DBRs is the ability to achieve lasing despite the 7.78% mismatched interface between the antimonide active

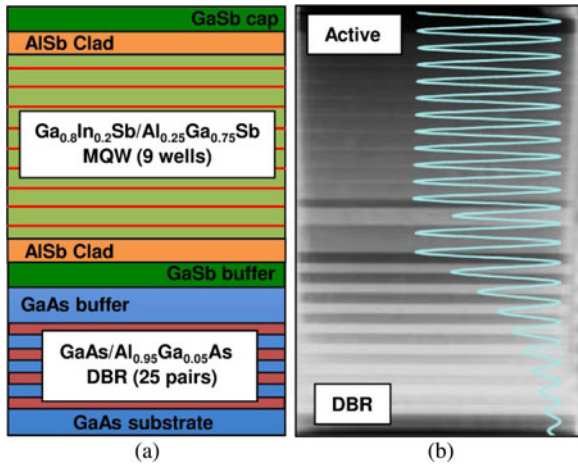


Fig. 2. (a) Schematic and (b) cross-sectional TEM image and plot of E-field for lattice mismatched 2- $\mu\text{m}$  III-Sb VECSEL grown on GaAs/AlGaAs DBR.

region and the arsenide-based DBR. The first QW is located within 500 nm of this highly mismatched interface. Thus, for such a VECSEL to work, the growth has to be optimized to achieve minimal threading dislocations in the active region and to achieve a reproducible relaxation of the metamorphic buffer.

### B. Interfacial Misfit Dislocation Array-Based Growth of GaSb on GaAs

The growth of the antimonide active regions on GaAs/AlGaAs DBRs is based on an interfacial layer of  $90^\circ$  misfit dislocations at the GaSb/GaAs growth interface. A key requirement for the VECSEL structure is that the array of  $90^\circ$  misfit dislocations forms reliably over large areas. The GaSb epilayer then spontaneously relaxes and has low TDD. This is important as threading dislocations would introduce a strong nonradiative recombination process in the QWs and relaxation that is not 100% would make the strain in the QWs unpredictable.

Researchers such as Rocher [5] have shown that such periodic misfit dislocation arrays exist beneath GaSb islands grown on GaAs substrates. These are  $90^\circ$  misfit dislocations arrays with the 56- $\text{\AA}$  periodicity corresponding to completely relaxed GaSb on GaAs. The growth of GaSb on GaAs is thus fundamentally different from the growth of similarly mismatched alloys such as InAs on GaAs. While InAs tends to grow in a Stransky–Krastanov growth mode where the coherent strain in the epilayer is relieved through the growth of 3-D nanostructures to manage the strain, the growth of GaSb proceeds in a spontaneous relaxation regime with the islands achieving close to 100% relaxation within the first few monolayer of growth. This periodic  $90^\circ$ -misfit dislocation array at the GaSb/GaAs interface is the primary mechanism for accommodating this mismatch. These periodic misfit dislocations spaced at  $\sim 56$   $\text{\AA}$  along both the  $[1\ 1\ 0]$  and  $[1\ -1\ 0]$  directions correspond to 13 lattice sites of GaSb or 14 lattice sites of GaAs. The 13:14 ratio between the GaSb and the GaAs lattice sites is the minimum value for the mismatch between the two lattice constants and can be interpreted as an energy minimization process that is achieved

through self-assembly or packing of Sb atoms on a GaAs surface.

Kaspi *et al.* [6] further identified and documented the fact that the TDD in the bulk growth of GaSb on GaAs arises from the coalescence of such islands. When two independent chains of periodic  $90^\circ$  dislocations merge, the periodicity of the misfit dislocations at the point of coalescence is lost, leading to the formation of  $60^\circ$ -misfit dislocations that have a very high probability of threading into the epilayer. Therefore, if the initial islands are larger and less numerous, the resulting bulk GaSb will have a lower TDD. The growth of the GaSb mismatched epilayers on GaAs was also investigated by Brar and Leonard [7] who for the first time showed the presence of extensive screw dislocations in the epilayer. These results were further investigated by Shanabrook *et al.* [8]. A typical non-IMF growth of GaSb on GaSb with screw dislocations is shown in Fig. 3(a). Thus, while the GaSb islands grown on GaAs are free of threading dislocations, the epilayer grown as a result of the coalescence of these islands has a TDD strongly correlated with the island density and more specifically with the number of coalescence sites.

Thus, to achieve low TDD of GaSb on GaAs, either the numbers of coalescence sites have to be significantly reduced or the arrays of  $90^\circ$  misfit dislocations under all islands have to be linked to form a coherent series. One method to form such a coherent series is to use an Sb ( $2 \times 8$ ) reconstruction on the GaAs surface prior to the growth of the GaSb epilayer. We have termed this reconstruction assisted interfacial misfit dislocation array. The reconstruction assisted interfacial misfit dislocation array is a fundamentally unique epitaxial growth mode based on atomic self-assembly of group V adatoms at a lattice mismatched interface [9]. The basic mechanism for the formation of such an interface is the realization of specific antimony surface reconstructions on the GaAs substrate. These are usually multilayer reconstructions such as the Sb ( $2 \times 8$ ) reconstruction that surpasses the critical thickness for the GaSb/GaAs material system without the actual growth of any GaSb. These multilayer antimony reconstructions are completely strain relieved and achieve this by forming the  $90^\circ$  misfit dislocations at the Sb/GaAs interface. The misfit dislocations are spaced uniformly 56  $\text{\AA}$  apart.

This 56- $\text{\AA}$  periodicity also corresponds to completely relaxed GaSb on GaAs since the spacing is equivalent to 13 lattice sites of GaSb or 14 of GaAs along the  $[1\ 1\ 0]$  and  $[1\ -1\ 0]$  directions and this can be shown to be the best possible ratio for relaxed GaSb on GaAs [10]. The atomic force micrograph (AFM) and cross-sectional TEM image of the IMF based growth of GaSb on GaAs are shown in Fig. 3(b) and (c), respectively. The AFM shows the complete elimination of screw dislocations, while the TEM shows the IMF array and a low TDD GaSb layer on GaAs. The reconstruction's ability to self-assemble and dynamically change its coverage on the substrate allows for a monolayer of completely relaxed GaSb to be realized across the GaAs substrate. At present, we have seen a network of such intact misfit dislocations across several square micrometers in area. In theory, such a periodic array should exist across the GaAs substrate regardless of its diameter. However, steps in the wafer

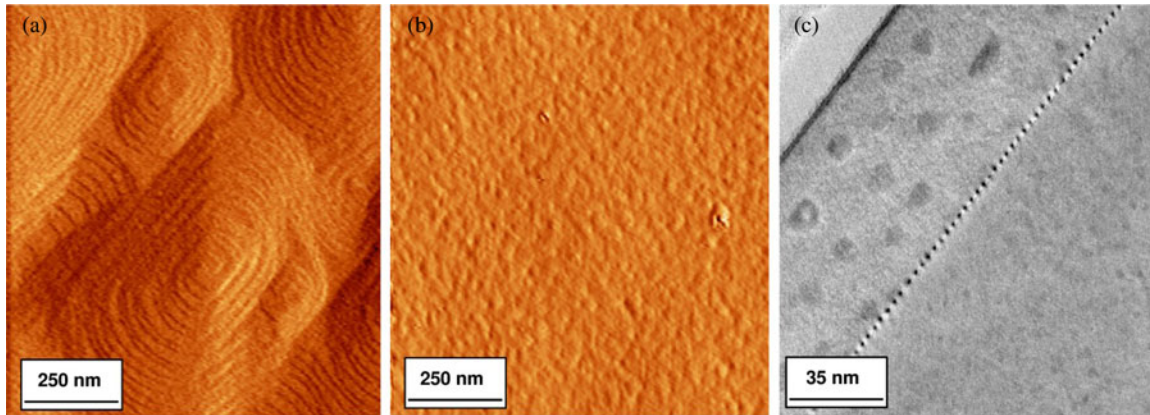


Fig. 3. (a) AFM of GaSb on GaAs without the formation of the IMF array. (b) AFM of GaSb on GaAs with an optimized IMF array at the GaSb/GaAs interface. (c) Cross-sectional TEM image of GaSb grown on GaAs with a periodic IMF array at the interface.

and arsenic intermixing in the Sb reconstruction have restricted these dislocation arrays to a few square micrometers in area, and threading dislocation densities of  $5 \times 10^6/\text{cm}^2$  has been observed [11]. The reduction in TDD is further evidenced by the published device results from this technique. This growth method has been used to demonstrate novel lasers and detectors based on the integration of antimonide lasers with GaAs and silicon substrates [12], [13].

### C. Optimization of IMF-Based QWs

The QW emission wavelength depends on the In content  $x$  and the thickness of the  $\text{Ga}_{1-x}\text{In}_x\text{Sb}$  QWs. At the typical growth temperatures (460–500 °C), the reevaporation of indium from the substrate is not negligible; thus, the actual In content of the QW material depends not only on the nominal In flux but also on the growth temperature. Furthermore, the QW emission wavelength and strength depends on its strain. The optical quality of the QWs depends on their growth temperature. Finally, the Sb flux supplied during growth of the active region becomes important with increasing III-Sb thickness, which is also growth temperature dependent. Thus, the QWs have to be optimized with respect to nominal In content, thickness, as well as growth temperature and Sb flux.

We use the photoluminescence (PL) intensity as an optimization parameter, as it is a good measure for the material's optical quality. Test samples with four QWs have been grown on GaAs, using the interfacial layer of  $90^\circ$  misfit dislocations. For comparison, test structures have also been grown directly on GaSb. Fig. 4 shows the PL of test structures with an 11-nm-thick  $\text{Ga}_{0.75}\text{In}_{0.25}\text{Sb}$  well, grown on GaAs and on GaSb. The PL intensity from the sample grown on GaAs exceeds the one from the sample grown directly on GaSb by 20%, indicating that the material's optical quality grown on GaAs is not significantly inferior to the material grown directly on GaSb. A simulated PL spectrum (Nonlinear Control Strategies Simulase software) shows good agreement with experimental data at  $T = 290$  K, carrier density  $N = 2.5 \times 10^{11} \text{ cm}^{-2}$ . However, small differences in strain between antimonide layers grown on GaAs with the interfacial layer of  $90^\circ$  misfit dislocations compared to those grown on GaSb can influence the strain in the QWs.

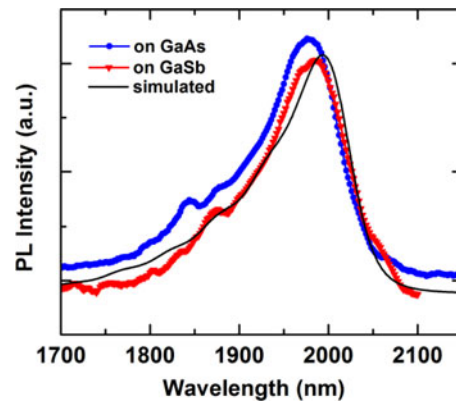


Fig. 4. PL of a structure with 11-nm-thick  $\text{Ga}_{0.75}\text{In}_{0.25}\text{Sb}$  QWs, grown on a GaAs substrate (blue), and grown on a GaSb (red). For comparison, a simulated PL spectrum for  $\text{Ga}_{0.75}\text{In}_{0.25}\text{Sb}$  QWs is included (black).

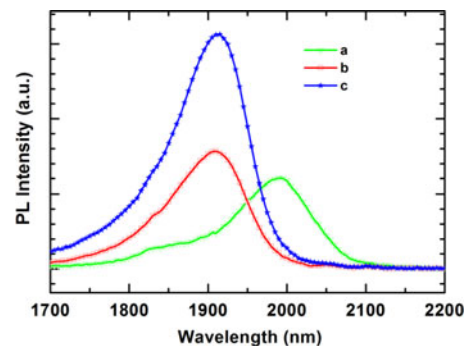


Fig. 5. PL of a structure with 10-nm-thick  $\text{Ga}_{0.72}\text{In}_{0.28}\text{Sb}$  QWs, grown at 475 °C (a), and at near 490 °C (b). For comparison, the emission wavelength of b can also be achieved by a structure with 12-nm-thick  $\text{Ga}_{0.8}\text{In}_{0.2}\text{Sb}$  well, grown at 475 °C (c).

This influences the optical emission from the III-Sb active region (PL peak wavelength and intensity), since it depends on the compressive strain in the QWs. Therefore, the active region for growth on GaAs has to be developed independently from that for growth on GaSb.

The growth temperature is controlled *in situ* by surface pyrometry. Fig. 5 shows the influence of the growth temperature. Samples *a* and *b* have nominally the same QWs (10-nm-wide

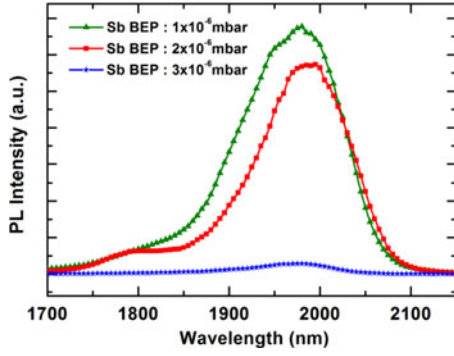


Fig. 6. Influence of the Sb flux, measured as beam equivalent pressure (BEP) on the PL of a VECSEL active region with nine QWs (grown on GaAs).

$\text{Ga}_{0.72}\text{In}_{0.28}\text{Sb}$ ), but are grown at different temperatures,  $475^\circ\text{C}$  and near  $490^\circ\text{C}$ , respectively. The emission wavelength of  $b$ , grown at higher temperature, is blue shifted by about 85 nm and is approximately 30% stronger than  $a$ . The blue shift can be attributed to In reevaporation, which increases at higher growth temperature. On the other hand, the shorter emission wavelength of  $b$  can also be achieved by growing a 12-nm-thick  $\text{Ga}_{0.8}\text{In}_{0.2}\text{Sb}$  well at  $475^\circ\text{C}$ , sample  $c$ , yielding more than twice the peak PL intensity. The 12-nm-thick  $\text{Ga}_{0.8}\text{In}_{0.2}\text{Sb}$  (sample  $c$ ) well contains less In than the 10-nm-wide  $\text{Ga}_{0.72}\text{In}_{0.28}\text{Sb}$  well (sample  $a$ ), which explains the wavelength shift between  $a$  and  $c$ . The change in intensity between samples  $b$  and  $c$  is due to differences in material quality, which depends on the growth temperature.

The optimal growth temperature of the QWs for an emission wavelength near  $2\ \mu\text{m}$  was determined to be  $470^\circ\text{C}$ . The layers prior to the first QW can be grown at higher temperature, e.g.,  $510^\circ\text{C}$  for the III-Sb, and  $580^\circ\text{C}$  for the III-As. Beginning with the first QW, all following layers must be grown at low temperature to avoid deterioration of the GaInSb QWs, an effect which unlike GaInAs QWs in III-As, will occur even if the temperature is increased after they are already buried in AlGaSb.

In the mismatched VECSEL, the III-Sb active region is grown on the GaAs/AlGaAs DBR. The DBR exhibits a slightly higher surface roughness compared to a GaAs substrate, which is associated with the Al-induced strain. It results in surface features elongated along the  $[0\ 1\ 1]$  direction. The average surface roughness is with 0.3-nm RMS  $\sim 50\%$  increased compared to a GaAs substrate. The increased surface roughness likely limits the formation of the  $90^\circ$  misfit dislocation array and potentially results in a higher density of threading dislocations compared to growth on smooth, epitaxial GaAs substrates.

For the growth of the entire active region with nine QWs, the optimization of the Sb flux during growth becomes important. The PL intensity increases by  $17\times$  when the Sb flux was reduced from  $3 \times 10^{-6}$  to  $1 \times 10^{-6}$  mbar (see Fig. 6). Generally, the PL intensity rises with lower Sb flux, until a minimum Sb flux, below which the substrate surface becomes group III rich and turns hazy. This minimum Sb flux depends on the growth temperature. The minimum Sb:Ga flux ratio is about 2.5 for growth temperatures near  $470^\circ\text{C}$ .

The PL optimization resulted in two QW designs: 10-nm  $\text{Ga}_{0.72}\text{In}_{0.26}\text{Sb}$  QWs in  $\text{Al}_{0.3}\text{Ga}_{0.7}\text{Sb}$  barriers and 13-nm

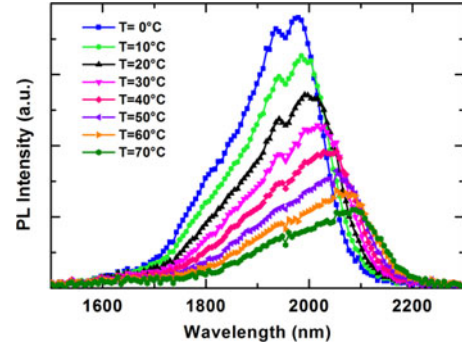


Fig. 7. Edge PL spectra from a VECSEL sample.

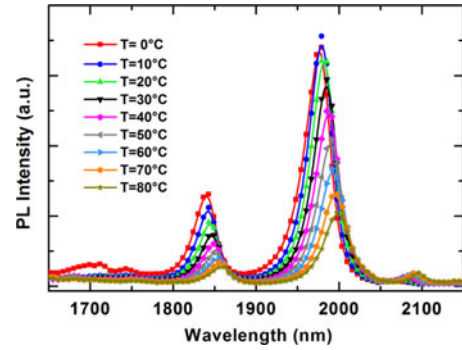


Fig. 8. Surface PL spectra from a VECSEL sample.

$\text{Ga}_{0.8}\text{In}_{0.2}\text{Sb}$  QWs in  $\text{Al}_{0.25}\text{Ga}_{0.75}\text{Sb}$  barriers. However, the latter design consistently led to superior laser performance.

#### D. VECSEL Growth Optimization

For optimized device performance, it is essential to precisely place the QWs at E-field antinodes within the subcavity. This requires precise control of growth rates of the group-III sources of MBE, as growth rate variation can affect both composition and thickness of the constituent layers. The growth rates are calibrated using reflection high-energy electron diffraction oscillations.

The QW gain region is characterized by its PL spectrum. The PL spectrum measured normal to the wafer surface is strongly modulated due to the subcavity etalon and the DBR. The edge-PL spectrum shows significantly weaker modulation and is, therefore, used to determine the QW emission's spectral peak position [1], [4], [14]. The VECSEL sample is mounted on a heat sink to measure the edge/surface PL spectrum at different heat-sink temperatures. Figs. 7 and 8 show edge and surface PL spectra from a VECSEL sample, respectively. The edge-PL shifts to longer wavelength at about 1.6 nm/K [14], primarily due to the bandgap energy dependence on temperature. The subcavity resonance also shifts to longer wavelength with increasing temperature, but more slowly when compared to the intrinsic gain peak shift, at about 0.26 nm/K. The subcavity resonance peak shift is due to temperature dependence of refractive indexes. The determination of gain peak and subcavity resonance shift with respect to temperature is useful for proper design of the VECSEL. To achieve high CW output power, the

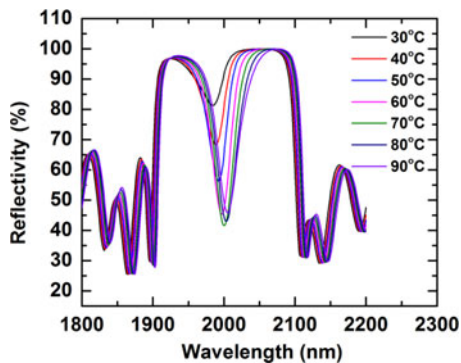


Fig. 9. Temperature-dependent reflectivity spectra from a VECSEL on GaAs/AlGaAs DBR.

gain peak emission is typically designed to be 30–50 nm shorter than the actual desired wavelength of device operation, such that the gain peak and subcavity resonance coincide at the desired operating temperature. The operating temperature depends on pump power, heat-sink temperature, and power dissipated in the active region.

The reflectivity spectrum is measured using a Fourier transform infrared spectrometer with the VECSEL chip mounted on a heat sink. Fig. 9 shows the reflectivity spectrum at different heat-sink temperatures. The reflectivity spectrum shows the effect of the subcavity etalon formed between DBR and air–semiconductor interface. The reflectivity spectrum is used to diagnose the deviation in thickness of layers and composition of both DBR and subcavity. For the reflectivity spectrum in Fig. 9, we observe that the most optimized overlap between intrinsic QW gain peak and subcavity resonance is at heat-sink temperature of 70 °C. This indicates a good agreement between the design and the epitaxially grown VECSEL sample.

### III. LASER CHARACTERIZATION

The VECSEL cavity is formed between DBR and an external output coupler. The output coupler radius of curvature  $R_{OC}$  and cavity length  $L$  is chosen to achieve optimal matching between optical mode and gain aperture size. The output coupler radius of curvature  $R_{OC}$  and cavity length  $L$  are related to gain-aperture size  $w$ ) of a linear cavity by [15]

$$w = \sqrt[4]{\frac{R_{OC}L\lambda^2 - L^2\lambda^2}{\pi^2}} \quad (1)$$

where  $\lambda$  is the wavelength. The pump spot size is adjusted to match the beam-waist size of the linear cavity as closely as possible by the two pump focussing lenses. For laser characterization of the VECSEL sample grown on GaAs, a linear cavity consisting of a curved output coupler (with  $R_{OC} = 70$ –100 mm and  $R \sim 99\%$ ) is used.

#### A. Pulsed Lasing Characterization

The VECSELS with III-Sb active regions and AlGaAs/GaAs DBRs were initially pumped optically by a pulsed source. This allows operation of the laser in a near subthermal regime without heat spreading elements. Fig. 10 shows the experimental setup.

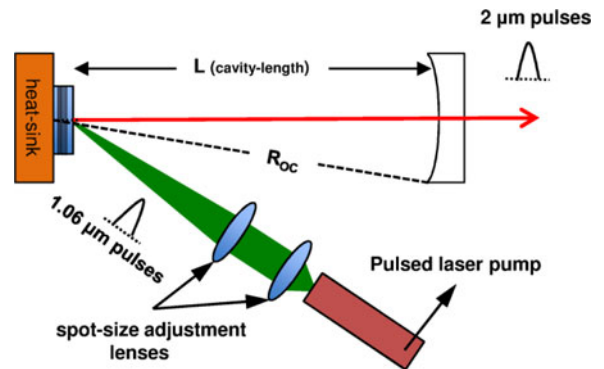


Fig. 10. Schematic for optically pumped VECSEL operated in pulsed mode.

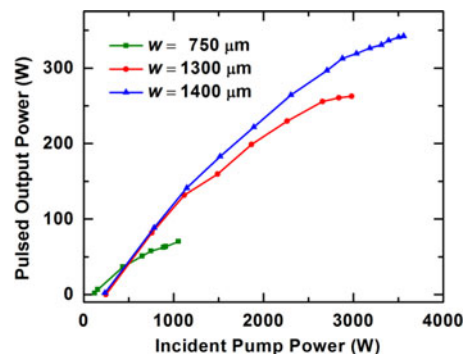


Fig. 11. Peak output power versus peak pump power for the pulsed III-Sb VECSEL on GaAs substrate.

The pump laser is a diode-pumped Nd:YAG laser. The repetition rate is 1 kHz and pulsewidth  $\tau_{\text{pulse}} \sim 300$  ns, with available peak power up to 1.2 kW. The diameter of pump spot is adjusted by varying the distance between the VECSEL chip and the pump-focusing lens.

Fig. 11 shows the pulsed peak output power versus peak pump power for a III-Sb VECSEL with AlGaAs/GaAs DBR. A linear cavity of length ( $L_c = 70$  mm) is used for pulsed lasing of the devices. The output coupler has  $R_{OC} = 100$  mm with reflectivity,  $R \sim 98\%$ . The threshold incident pump power density is calculated to be 17.44 kW/cm<sup>2</sup>. The peak output power from this device has been reported as high as 340 W [16].

#### B. CW Lasing Characterization

The initial CW lasing characterization is done using an intracavity heat spreader (transparent diamond or silicon carbide, SiC); the setup is shown in Fig. 12. The fabrication of the VECSEL from the epitaxially grown sample begins with thinning the substrate to  $\sim 100$   $\mu\text{m}$ ; it is then soldered onto a heat sink using thin indium foil with gold metallization. In order to dissipate heat generated in the active region, a transparent heat spreader is attached to the epise of the sample by means of capillary bonding.

Fig. 13 shows the  $L$ – $L$  characteristics for the VECSEL device grown on GaAs/AlGaAs DBR for heat-sink temperatures in the range of  $-5$  to 20 °C. A 980-nm fiber coupled diode laser is used for photopumping of this VECSEL device. The device is

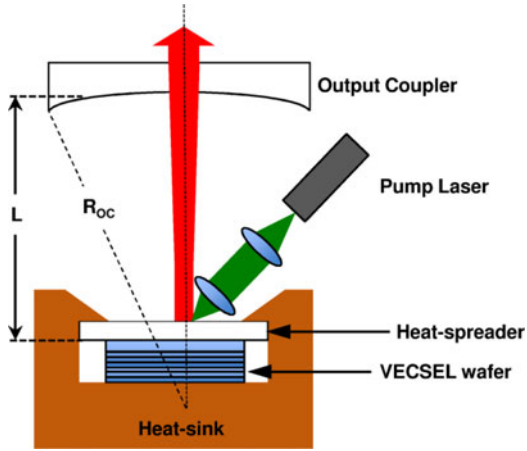


Fig. 12. Schematic for optically pumped VECSEL operated in CW mode.

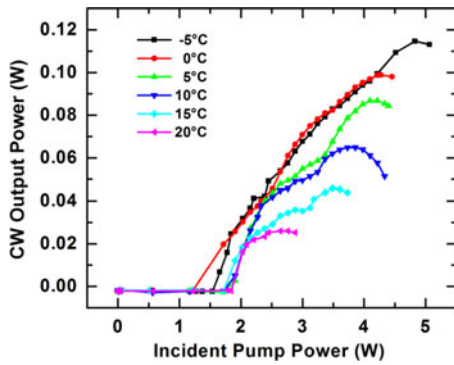


Fig. 13. Output power versus pump power for the CW III-Sb VECSEL on GaAs substrate.

pumped at an incident angle of  $30^\circ$  with a pump spot size of  $w = 130 \mu\text{m}$ . SiC is used as an intracavity transparent heat spreader on the episcrface. The threshold incident pump power density  $P_{\text{th}}$  is calculated to be  $13.9 \text{ kW/cm}^2$  for the laser operating at  $20^\circ\text{C}$  [17]. The maximum CW output power is observed to be  $\sim 120 \text{ mW}$  at a heat-sink temperature of  $-5^\circ\text{C}$ . A similar setup is used for characterizing the lattice matched III-Sb VECSEL.

#### IV. DISCUSSIONS

##### A. Effect of Mismatched Epitaxy on VECSEL Performance

The lattice mismatched III-Sb laser with GaAs/AlGaAs DBRs has a very similar structure to their lattice matched counterparts. However, the performance of the antimonide VECSELS on GaAs is significantly inferior compared to the lattice matched VECSELS on GaSb. This can be seen in Table I which shows the key metrics for a lattice mismatched III-Sb VECSEL on GaAs/AlGaAs DBR versus those for a lattice matched VECSEL grown on GaSb.

The mismatched VECSEL's threshold pump power density is with  $13.9 \text{ kW/cm}^2$  much higher than  $1.19 \text{ kW/cm}^2$  for the lattice matched VECSEL. Furthermore, there is also a significant decrease in the wall-plug efficiency and the maximum CW output power obtained from the lattice mismatched laser grown on GaAs/AlGaAs DBR. It can be speculated that the deterioration

TABLE I  
PERFORMANCE COMPARISON OF LATTICE MISMATCHED III-Sb VECSEL ON GaAs/AlGaAs TO LATTICE MATCHED VECSEL ON GaSb/AlAsSb

Device	$\eta_d$ (%)	$P_{\text{th}}$ (kW/cm <sup>2</sup> )	$P_{\text{max}}$ (W)
III-Sb VECSEL on GaAs/AlGaAs DBR	3.5	13.9	0.12
III-Sb VECSEL on GaSb/AlAsSb DBR	14.1	1.19	2.95

in the performance of the VECSEL when grown mismatched on GaAs compared to when it is grown lattice matched on GaSb can be attributed to the presence of threading dislocations in the active region when it is grown on the GaAs/AlGaAs DBR.

The carrier loss equation in VECSEL structures can be expressed as follows [18]:

$$R_{\text{loss}} = R_{\text{Defect}} + R_{\text{SE}} + R_{\text{Auger}} + R_{\text{remaining}} \quad (2)$$

where  $R_{\text{loss}}$  is the carrier loss equation rate,  $R_{\text{Defect}}$  is the carrier loss equation rate due to carrier recombination via defect states,  $R_{\text{SE}}$  is the loss due to spontaneous emission processes,  $R_{\text{Auger}}$  is the carrier loss due to Auger recombination processes, and  $R_{\text{remaining}}$  is the carrier loss due to carriers not captured by wells or tunnelled carriers not recaptured in other wells. A widely accepted model to represent such losses is also known as ‘‘ABC’’ model:

$$R_{\text{loss}} = N/\tau_d + BN^2 + CN^3 + R_{\text{remaining}} = N/\tau \quad (3)$$

where  $\tau$  is the carrier lifetime under low carrier concentration (no stimulated emission), and  $\tau_d$  is the inverse of the Shockley–Read–Hall coefficient  $A$ . In VECSEL structures,  $R_{\text{remaining}}$  is typically neglected, since most of the carriers generated in the barrier region are captured in the QWs with high probability, and carrier capturing is also enhanced by the AlSb carrier confinement layers. However, the ‘‘ABC’’ empirical model is not adequate to model the carrier losses at high carrier density and high temperature (typical operating conditions of a high-power VECSEL). A fully microscopic many-body approach used for computation of losses has shown a better agreement between experimental and theoretical data [19], [20]. Therefore, the carrier loss equation can be represented as follows:

$$R_{\text{loss}} = N/\tau_d + R_{\text{SE}}(N, T) + R_{\text{Auger}}(N, T) = N/\tau \quad (4)$$

where  $R_{\text{SE}}$  and  $R_{\text{Auger}}$  are functions of carrier density and operating temperature of the device. One way to determine losses in the structure is by measuring the internal quantum efficiency. The internal quantum efficiency is defined as the ratio of carrier recombination rate through spontaneous emission to total number of absorbed pump photons:  $\eta_i = R_{\text{SE}}/R_{\text{loss}}$ . The defect recombination coefficient is estimated to be  $\tau_d = 2.6 \text{ ns}$  for III-Sb VECSEL structures grown on GaAs/AlGaAs DBRs. The  $\tau_d$  for the III-Sb VECSEL structure grown on GaSb substrates is determined to be  $16 \text{ ns}$  [14]. The low value of  $\tau_d$  for the lattice mismatched VECSEL structure grown on the GaAs/AlGaAs

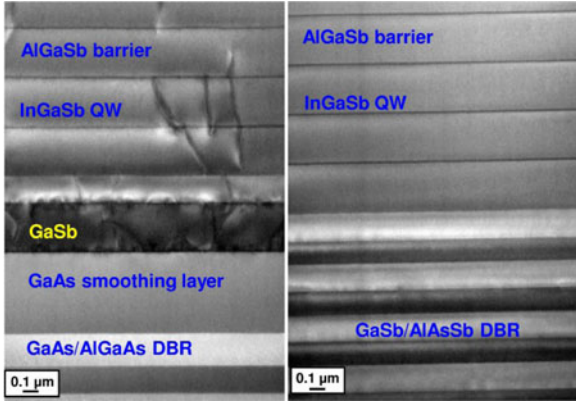


Fig. 14. TEM comparison of lattice mismatched III-Sb VECSEL on GaAs/AlGaAs to lattice matched VECSEL on GaSb/AlAsSb. (a) Lattice mismatched structure with extensive threading dislocations in the active region and (b) complete absence of threading dislocations in the lattice matched structure.

DBR can be attributed to the presence of dislocations in the active region. These defects can act as nonradiative recombination centers. Thus, the source of the threading dislocations and their density in the active region should be investigated.

### B. TEM-Based Analysis of TDD in the VECSELS

The investigation of the TDD in the III-Sb VECSELS involves cross-sectional TEM analysis of both the lattice mismatched and the lattice matched III-Sb VECSELS. These VECSELS are cross-sectioned with a focused ion beam lift out using an FEI Helios 450 DIB system. The TEM images were taken using an FEI Tecnai F20 equipped with HAADF STEM detector. For the initial TEM/STEM imaging, the samples were  $\sim 150$  nm thick near the top of the active region and  $\sim 250$  nm thick near the active region/DBR interface.

The images of the lattice mismatched and the lattice matched antimonide VECSELS are shown in Fig. 14. In the case of the III-Sb VECSEL on GaAs/AlGaAs DBR, the strain from the lattice mismatch is to be relieved at the (GaSb/GaAs) interface through misfit dislocations [9]. However, in many cases, there are breaks and discontinuities associated with the IMF interface, when grown on the GaAs/AlGaAs DBR compared to the IMF interface on GaAs substrates. This leads to threading dislocations at these discontinuities as can be seen in Fig. 14(a). Furthermore, these threading dislocations reach into the QW active region and are the source for the nonradiative recombination in the lasers and the reduced  $\tau_d$  values. Fig. 14(b) shows the high-resolution cross-sectional TEM image for the lattice matched VECSEL. This image shows the no-threading dislocations in the active region.

From the X-TEM image of the III-Sb VECSEL structure on GaAs/AlGaAs DBR, it is evident that the active region contains a significant density of dislocations. The presence of dislocations within the carriers' diffusion length leads to a reduction in carrier lifetime. The carrier lifetime is related to the dislocation density  $N_D$  by the following formula [21]:

$$\frac{1}{\tau_d} = \frac{\pi^2 \mu k T N_D}{4q} \quad (5)$$

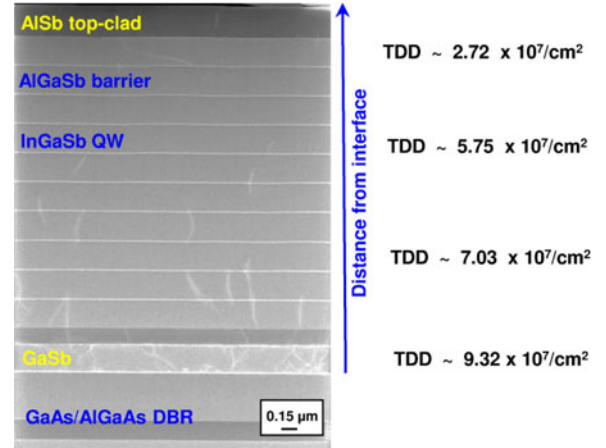


Fig. 15. STEM image of lattice mismatched III-Sb VECSEL on GaAs/AlGaAs showing the source of the threading dislocations at the IMF array and subsequent reduction in the density as a function of distance from the mismatched interface.

where  $\tau_d$  is the carrier lifetime associated with recombination assisted by dislocations,  $\mu$  is the carrier mobility, and  $q$  is the electronic charge. The overall carrier lifetime  $\tau$  is then

$$\frac{1}{\tau} = \frac{1}{\tau_0} + \frac{1}{\tau_d} \quad (6)$$

where  $\tau_0$  is the carrier lifetime in dislocation free material. The carrier lifetime in the lattice matched III-Sb VECSEL is close to  $\tau_0$ , as it is almost free of dislocations, as can be seen in the high-resolution TEM image. In a TEM image, one can measure the total projected length in the TEM image plane of dislocation lines  $l'$ . The dislocation density can then be estimated using the following equation [22]:

$$N_D = \frac{4}{\pi} \frac{l'}{At} \quad (7)$$

where  $t$  is the sample thickness and  $A$  is the area over which the projected length  $l'$  is estimated.

In Fig. 15, we estimate the dislocation density  $N_D$  as a function of distance from the GaSb/GaAs interface. The dislocation density reduces from  $\sim 10^8$  to about  $\sim 10^7$   $\text{cm}^{-2}$  at a distance of about  $3 \mu\text{m}$  from the interface. Thus, it is evident from the relationship between carrier lifetime and dislocation density (6) that the higher TDD found in the III-Sb VECSELS grown lattice mismatched on GaAs/AlGaAs DBRs is detrimental to the VECSEL performance [14]. Furthermore, this high TDD in the III-Sb on GaAs/AlGaAs can also be linked to the high threshold density, lower efficiency, and reduced maximum output power compared to a lattice matched III-Sb VECSEL.

### V. THREADING DISLOCATION REDUCTION STRATEGIES

The detrimental effect of the high TDD in the mismatched VECSEL's active region requires strategies for either reducing these dislocations or bending the dislocations before they can reach the active regions. One option is to improve the IMF interface when the GaSb is grown on GaAs/AlGaAs DBR and

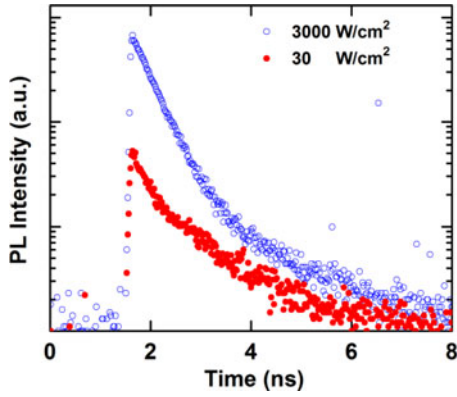


Fig. 16. Transient PL decay measured on QWs grown with IMF with the average excitation powers of 30 and 3000  $\text{W}/\text{cm}^2$ .

the second approach is to move the IMF interface further away from the active region.

#### A. Optimizing the IMF Layer Using Time-Resolved PL Measurements

The TEM analysis of the III-Sb active regions on GaAs/AlGaAs DBR provides proof about the existence of threading dislocations in the proximity of the QWs. However, to optimize the IMF interface itself, we require an alternate technique that can be used to characterize the interface more systematically. The optical properties of III-Sb active regions grown on GaAs with and without IMF interface are compared by time-resolved PL. While we are yet to make use of this process to optimize QWs for the VECSEL active region, we have been able to demonstrate this approach to establish the effectiveness of the IMF interface on III-Sb active regions grown on GaAs substrates. For this purpose, we have grown two QW samples on (0 0 1) GaAs substrates. Both samples have the same twin QW structures, i.e., 50-nm  $\text{Al}_{0.5}\text{Ga}_{0.5}\text{Sb}$  barrier/8-nm GaSb well/50-nm  $\text{Al}_{0.5}\text{Ga}_{0.5}\text{Sb}$  barrier/8-nm GaSb well/50-nm  $\text{Al}_{0.5}\text{Ga}_{0.5}\text{Sb}$  barrier/5-nm GaSb cap grown on 100-nm GaSb buffer layer. One sample was grown with the IMF at the GaSb/GaAs interface and the other without the IMF.

Time-resolved measurements were performed employing a Ti:Sapphire mode-locked laser generating 5-ps laser pulses tuned at 1.55 eV (800 nm) at the repetition rate of 76 MHz. The laser pulses were focused on the sample surface kept at 4 K in a liquid-He circulating cryostat via an objective lens with the numerical aperture of 0.42. Luminescence from the sample was collected with the same objective lens and was detected with a near-infrared streak camera (Hamamatsu C11293-01) combined with a 150-grooves/mm monochromator. The measurement time resolution was 20 ps.

The measured PL time decay was spectrally integrated at each transient time and the integrated intensities are shown in Fig. 16. The two sets of data are displayed for the average excitation power densities of 30 and 3000  $\text{W}/\text{cm}^2$ . The measured transient PL intensities were generally well fitted with the double exponential function of  $I(t) = I_{\text{dark}} + A_1 \exp(-t/\tau_1) + A_2 \exp(-t/\tau_2)$ , where  $I_{\text{dark}}$  is the dark counts without the

TABLE II  
PARAMETERS DETERMINED FROM THE FITTING TO THE TRANSIENT PL DECAY

Excitation Power ( $\text{W}/\text{cm}^2$ )	QW with IMF			QW without IMF		
	$A_1/A_2$	$\tau_1$ (ps)	$\tau_2$ (ps)	$A_1/A_2$	$\tau_1$ (ps)	$\tau_2$ (ps)
30	4.47	1006 $\pm$ 21	222 $\pm$ 6	6.78	1560 $\pm$ 20	250 $\pm$ 8
150	3.46	1000 $\pm$ 14	260 $\pm$ 7	6.44	1530 $\pm$ 27	243 $\pm$ 7
750	3.55	1050 $\pm$ 17	310 $\pm$ 7	6.23	1450 $\pm$ 30	248 $\pm$ 5
1550	2.98	1004 $\pm$ 20	330 $\pm$ 10	6.79	1550 $\pm$ 26	258 $\pm$ 7
3000	2.69	1019 $\pm$ 28	351 $\pm$ 8	6.58	1590 $\pm$ 19	257 $\pm$ 9

pulsed laser excitation,  $A_1$  and  $A_2$  are the amplitudes of each term, and  $\tau_1$  and  $\tau_2$  are the decay time constants. These parameters were determined by the fittings shown by the solid lines in Fig. 16 and are summarized in Table II. To identify the origin of the two decay time constants of  $\tau_1$  and  $\tau_2$ , we have studied the time decay by spectral integrations in limited ranges [23]. For example, the PL decay measured on the QW with IMF was spectrally separated into the two regions of 1367–1405 nm (882–907 meV) and 1406–1444 nm (859–882 meV) and integrated in each region. This spectral separation resulted in single exponential decays and the decay time constants determined in the lower and higher photon energy regions very nicely reproduced the  $\tau_1$  and  $\tau_2$  values given in Table II, respectively [23]. Therefore,  $\tau_1$  and  $\tau_2$  are the decay time constants related to the QW ground states and the excited states, respectively.

The comparison of the two sets of data in Table II on the QWs with and without IMF shows a clear difference of the excitation power dependence of the  $\tau_2$  value. With IMF, the  $\tau_2$  value and the amplitude  $A_2$  increased with the excitation power, while they were independent of the excitation power without IMF. After the pulsed laser excitation of the QW samples, the excited electrons and holes experience energy relaxation. Therefore, the  $\tau_2$  value of the excited states includes this energy relaxation process and is much shorter than the  $\tau_1$  value of the ground states. The increase of the excitation power generally enhances the band filling of the QW ground states with the photogenerated carriers, and this reduces the energy relaxation rate in both the conduction and valence bands due to the filling of the energy states above the band edges. This will result in the increase of the  $\tau_2$  value for the QW with IMF. The enhanced steep decay in Fig. 16 for the higher excitation corresponds to the increase of the amplitude  $A_2$ . The fact that the QW without IMF did not show any excitation power dependence indicates the presence of residual defects that prevent the band filling effect in the QW ground states.

The difference of the band filling effect is also clear from the measured PL spectra. The inset of Fig. 17 is the PL spectra measured with the CW excitation power of 2500  $\text{W}/\text{cm}^2$ . The peak shift with the excitation power is plotted in Fig. 17. While the PL peaks in both QWs were observed at around 870 meV for the lower excitation power, the clear difference of the blue shift was observed at the higher excitations. The PL peak steadily blue shifts for the QW with IMF, indicating band filling, while the spectral shift is less significant for material without an IMF interface. This difference is consistent with the above discussions

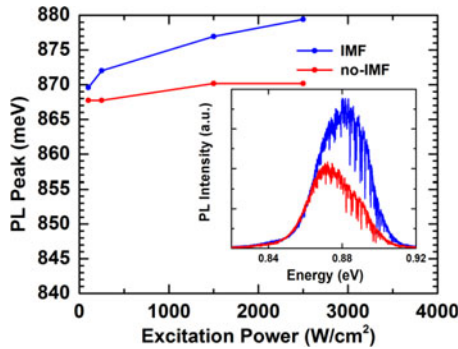


Fig. 17. PL peak shift with the excitation power. Clear blue shift is observed with QW with IMF. Inset shows the PL spectra measured at the excitation power of 2500 W/cm<sup>2</sup> on QWs grown with IMF and without IMF.

on the PL decay time constants. From the present PL measurements, we conclude that the QW with IMF exhibits superior optical properties with the reduction of the defects originating from the GaSb/GaAs highly mismatched heterointerfaces.

## VI. CONCLUSION

We have demonstrated the growth and characterization of 2- $\mu$ m III-Sb VECSELs on GaAs/AlGaAs DBRs with an active region consisting of nine InGaSb/AlGaSb QWs. The VECSELs consist of an III-Sb active region with the lattice constant of GaSb ( $a = 6.09$  Å) and a GaAs/AlGaAs DBR with the lattice constant of GaAs ( $a = 5.65$  Å). The 7.78% mismatched is lattice constant is managed by establishing an array of 90° misfit dislocations attaining  $\sim 100\%$  relaxation of the GaSb layer and achieving a significant reduction in TDD. The VECSELs have been optimized for several parameters including the QWs and the thickness of the individual layers. The III-Sb VECSELs on GaAs/AlGaAs DBRs were characterized for lasing performance under both subthermal pulsed conditions and CW conditions. The maximum output power obtained from mismatched VECSELs under pulsed and CW lasing conditions is 340 W and 120 mW, respectively. The threshold pump density, efficiency, and the maximum output power of the mismatched VECSELs were reduced compared to fully lattice matched III-Sb VECSELs. An analysis of the active region quality was conducted using TEM, which established the presence of extensive threading dislocations in the active region grown on the GaAs/AlGaAs DBR. Time-resolved PL measurements show superior optical properties for IMF grown III-Sb active regions on GaAs than for those grown without IMF interface.

## REFERENCES

- [1] O. G. Okhotnikov, *Semiconductor Disk Lasers: Physics and Technology*. Weinheim, Germany: Wiley, Apr. 2010.
- [2] B. Heinen, T. L. Wang, M. Sparenberg, A. Weber, B. Kunert, J. Hader, S. W. Koch, J. V. Moloney, M. Koch, and W. Stolz, "106 W continuous-wave output power from vertical-external-cavity surface-emitting laser," *Electron. Lett.*, vol. 48, no. 9, pp. 516–517, Apr. 2012.
- [3] M. Y. A. Raja, S. R. J. Brueck, M. Osinski, C. F. Schaus, and J. G. McInerney, "Novel wavelength-resonant optoelectronic structure and its application to surface-emitting semiconductor lasers," *Electron. Lett.*, vol. 24, no. 18, pp. 1140–1142, Sep. 1988.
- [4] A. C. Tropper and S. Hoogland, "Extended cavity surface-emitting semiconductor lasers," *Prog. Quantum Electron.*, vol. 30, no. 1, pp. 1–43, Jan. 2006.
- [5] A. M. Rocher, "Interfacial dislocations in the GaSb/GaAs (0 0 1) heterostructure," *Solid State Phenomena*, vol. 19/20, pp. 563–572, Jan. 1991.
- [6] W. Qian, M. Skowronski, and R. Kaspi, "Dislocation density reduction in GaSb films grown on GaAs substrates by molecular beam epitaxy," *J. Electrochem. Soc.*, vol. 144, no. 4, pp. 1430–1434, Jan. 1997.
- [7] B. Brar and D. Leonard, "Spiral growth of GaSb on (0 0 1) GaAs using molecular beam epitaxy," *Appl. Phys. Lett.*, vol. 66, no. 4, pp. 463–465, Jan. 1995.
- [8] B. R. Bennett, R. Magno, and B. V. Shanabrook, "Molecular beam epitaxial growth of InSb, GaSb, and AlSb nanometer-scale dots on GaAs," *Appl. Phys. Lett.*, vol. 68, no. 4, pp. 505–507, Jan. 1996.
- [9] S. H. Huang, G. Balakrishnan, A. Khoshakhlagh, A. Jallipalli, L. R. Dawson, and D. L. Huffaker, "Strain relief by periodic misfit arrays for low defect density GaSb on GaAs," *Appl. Phys. Lett.*, vol. 88, no. 13, pp. 131911-1–131911-3, Mar. 2006.
- [10] A. Jallipalli, G. Balakrishnan, S. H. Huang, A. Khoshakhlagh, L. R. Dawson, and D. L. Huffaker, "Atomistic modeling of strain distribution in self-assembled interfacial misfit dislocation (IMF) arrays in highly mismatched III-V semiconductor materials," *J. Cryst. Growth*, vol. 303, no. 2, pp. 449–455, May 2007.
- [11] M. Mehta, A. Jallipalli, J. Tatebayashi, M. N. Kutty, A. Albrecht, G. Balakrishnan, L. R. Dawson, and D. L. Huffaker, "Room-temperature operation of buffer-free GaSb–AlGaSb quantum-well diode lasers grown on a GaAs platform emitting at 1.65  $\mu$ m," *IEEE Photon. Technol. Lett.*, vol. 19, no. 20, pp. 1628–1630, Oct. 2007.
- [12] T. Yang, L. Lu, M. Shih, J. D. O'Brien, G. Balakrishnan, and D. L. Huffaker, "Room temperature InGaSb quantum well microcylinder lasers at 2  $\mu$ m grown monolithically on a silicon substrate," *J. Vac. Sci. Technol.*, vol. 5, no. 5, pp. 1622–1625, Sep. 2007.
- [13] A. Jallipalli, M. N. Kutty, G. Balakrishnan, J. Tatebayashi, N. Nuntawong, S. H. Huang, L. R. Dawson, D. L. Huffaker, Z. Mi, and P. Bhattacharya, "1.54  $\mu$ m GaSb/AlGaSb multi-quantum-well monolithic laser at 77 K grown on miscut Si substrate using interfacial misfit arrays," *Electron. Lett.*, vol. 43, no. 22, pp. 1198–1199, Oct. 2007.
- [14] A. Laurain, J. Hader, Y. Y. Lai, T. L. Wang, M. Yarborough, G. Balakrishnan, T. J. Rotter, P. Ahirwar, and J. V. Moloney, "Influence of non-radiative carrier losses on pulsed and continuous VECSEL performance," in *Proc. Soc. Photo-Opt. Instrum. Eng.*, 2012, vol. 8242, p. 82420S.
- [15] A. R. Albrecht, "InAs quantum dot vertical-cavity lasers," Ph.D. dissertation, Dept. Phys. Astron., Univ. New Mexico, Albuquerque, USA, 2009.
- [16] Y. Y. Lai, J. M. Yarborough, Y. Kaneda, J. Hader, J. V. Moloney, T. J. Rotter, G. Balakrishnan, C. Hains, and S. W. Koch, "340-W peak power from a GaSb 2- $\mu$ m optically pumped semiconductor laser (OPSL) grown mismatched on GaAs," *IEEE Photon. Technol. Lett.*, vol. 22, no. 16, pp. 1253–1255, Aug. 2010.
- [17] T. J. Rotter, J. Tatebayashi, P. Senanayake, G. Balakrishnan, M. Rattunde, J. Wagner, J. Hader, J. V. Moloney, S. W. Koch, L. R. Dawson, and D. L. Huffaker, "Continuous-wave, room-temperature operation of 2- $\mu$ m Sb-based optically-pumped vertical-external-cavity surface-emitting laser monolithically grown on GaAs substrates," *Appl. Phys. Exp.*, vol. 2, no. 11, pp. 112102-1–112102-3, Nov. 2009.
- [18] J. Hader, J. V. Moloney, S. W. Koch, L. Fan, and M. Fallahi, "Carrier recombination in semiconductor lasers: Beyond the ABC," in *Proc. Int. Conf. Numerical Simul. Semicond. Optoelectron Devices*, 2006, pp. 39–40.
- [19] J. Hader, G. Hardesty, T.-L. Wang, M. J. Yarborough, Y. Kaneda, J. V. Moloney, B. Kunert, W. Stolz, and S. W. Koch, "Predictive microscopic modeling of VECSELs," *IEEE J. Quantum Electron.*, vol. 46, no. 5, pp. 810–817, May 2010.
- [20] J. Hader, J. V. Moloney, and S. Koch, "Microscopic evaluation of spontaneous emission- and Auger-processes in semiconductor lasers," *IEEE J. Quantum Electron.*, vol. 41, no. 10, pp. 1217–1226, Oct. 2005.
- [21] J. E. Ayers, "Properties of semiconductors," in *Heteroepitaxy of Semiconductors: Theory, Growth, and Characterization*. Boca Raton, FL, USA: CRC Press, Jan. 2007, ch. 2, pp. 7–74.
- [22] T. W. Butler, "On the determination of dislocation densities," USNA Eng. Dept., Annapolis, MD, USA, Rep. E-69–1, May 1969.
- [23] N. A. Jahan, P. Ahirwar, T. J. Rotter, G. Balakrishnan, H. Kumano, and I. Suemu, "Spectral and transient luminescence measurements on GaSb/AlGaSb multiple quantum wells grown on GaSb/GaAs heterojunctions with and without interfacial misfit arrays," *Jpn. J. Appl. Phys.*, submitted for publication.



**Pankaj Ahirwar** received the undergraduate degree in electrical engineering from the Indian Institute of Technology Roorkee, Roorkee, India, in 2005. He is currently working toward the Ph.D. degree in the Department of Electrical and Computer Engineering, The University of New Mexico, Albuquerque, USA.

His research interests include the epitaxial development and characterization of vertical external cavity surface-emitting lasers based on antimonide active regions.



**Thomas J. Rotter** (M'07) received the M.S. degree in physics from the Westphaelische Wilhelms-Universitaet, Muenster, Germany, in 1997, and the Ph.D. degree in optical sciences from The University of New Mexico (UNM), Albuquerque, USA, in 2007.

From 2007 to 2009, he was a Research Scientist at the California NanoSystems Institute, The University of California, Los Angeles, USA. In 2009, he joined the Center for High Technology Materials at UNM as a Research Assistant Professor. His current research interests include epitaxy and characterization

of III-V arsenides, antimonides, and phosphides including highly mismatched materials and self-assembled nanostructures for optical applications, in particular high-power surface-emitting lasers.

Dr. Rotter is a member of the Optical Society of America and the Deutsche Physikalische Gesellschaft (German Physical Society).

**Darryl Shima**, photograph and biography not available at the time of publication.



**Nahid A. Jahan** received the B.Sc. and M.Sc. degrees from the Department of Applied Physics and Electronic Engineering, Rajshahi University, Rajshahi, Bangladesh, in 2005 and 2007, respectively. She is currently working toward the Ph.D. degree at the Graduate School of Information Science and Technology, Hokkaido University, Sapporo, Japan.

Her research interests include the study of electronic and optical properties of the III-V semiconductor heterostructures most preferably for the investigation of carrier leakage and dynamics in quantum

wells and dots.



**Stephen P. R. Clark** received the B.S. degree in chemical engineering with a concentration in materials science from The University of New Mexico, Albuquerque, USA, where she is currently working toward the Ph.D. degree in the Nanoscience Microsystems Program.

His current research interests include epitaxy and characterization of III-V arsenides and antimonides for novel nanostructures in applications in high-powered lasers and high-efficiency solar cells.

**Sadhvikas J. Addamane** is currently working toward the undergraduate degree in the Department of Electrical Engineering, The University of New Mexico (UNM), Albuquerque, USA.

His research interests include epitaxial growth and characterization of III-V materials.



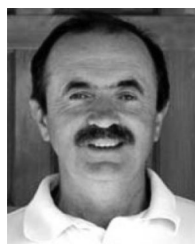
**Ganesh Balakrishnan** (M'07) received the B.E. degree in electronics and communications engineering from the University of Madras, Chennai, India, in 2000, the M.S. degree in engineering with a specialization in communication engineering from the University of Toledo, Toledo, OH, USA, in 2001, and the Ph.D. degree in optical sciences from The University of New Mexico (UNM), Albuquerque, USA, in 2006.

He is currently an Assistant Professor at the Center for High Technology Materials, UNM. He has coauthored 46 journal articles and more than 50 conference presentations. His research interests include high-power vertical external-cavity surface-emitting laser development using quantum dot based and antimonide quantum-well-based active regions.

**Alexandre Laurain**, photograph and biography not available at the time of publication.

**Jörg Hader**, photograph and biography not available at the time of publication.

**Yi-Ying Lai**, photograph and biography not available at the time of publication.



**Jerome V. Moloney** received the B.Sc. degree from the University College Cork, Cork, Ireland, in 1970, and the Ph.D. degree from the University of Western Ontario, London, ON, Canada, in 1976.

He was a Research Associate at the Universität Bielefeld, Bielefeld, Germany, from 1977 to 1979. He then joined the Optical Sciences Center, University of Arizona, Tucson, USA, in 1979, as a Research Associate. From 1981 to 1984, he was a Research Assistant Professor and Research Associate Professor.

In 1984, he became a Lecturer at Heriot Watt University, Edinburgh, U.K., and was promoted to Reader in 1986. He is currently a Full Professor of mathematics and optical sciences and the Director of the Arizona Center for Mathematical Sciences, University of Arizona. His current research interests include building a first principles theory of semiconductor lasers and ultrashort high-power pulse propagation in air.



**Ikuro Suemune** received the Doctoral degree in physical electronics from the Tokyo Institute of Technology, Tokyo, Japan, in 1977.

In April 1993, he joined the Research Institute for Electronic Science, Hokkaido University, Sapporo, Japan, where he is currently a Professor. He leads the Nanophotonics Laboratory, which is now located in the Green-nanotechnology Research Center, Hokkaido University. He has authored or coauthored 310 refereed journal publications, more than 50 invited talks in international conferences, and more than 15 invited book chapters. His major research interests include single-dot spectroscopy and "superconducting photonics."

**Robert G. Bedford**, photograph and biography not available at the time of publication.